Silver Accumulation in the Green Microalga Coccomyxa actinabiotis: Toxicity, in Situ Speciation, and Localization Investigated Using Synchrotron XAS, XRD, and TEM

Leonardo, T.; Farhi, E.; Pouget, S.; Motellier, S.; Boisson, A. M.; Banerjee, D.; Rebeille, F.; Den Auwer, C.; Rivasseau, C.;

Originally published:

November 2015

Environmental Science & Technology 50(2016), 359-367

DOI: https://doi.org/10.1021/acs.est.5b03306

Silver accumulation in the green microalga *Coccomyxa actinabiotis*: toxicity, *in situ* speciation and localization investigated using synchrotron XAS, XRD and TEM

Thomas Leonardo[1,2], Emmanuel Farhi[2], Stéphanie Pouget[3], Sylvie Motellier[4], Anne-Marie Boisson[1], Dipanjan Banerjee[5], Fabrice Rébeillé[1], Christophe den Auwer[6], and Corinne Rivasseau[1]*

[1]CEA, DSV, Laboratoire de Physiologie Cellulaire Végétale, 17 rue des Martyrs, 38054 Grenoble, France. CNRS, UMR5168, 38054 Grenoble, France. Université de Grenoble, 38000 Grenoble, France. INRA, 38054 Grenoble, France.

[2]Institut Laue Langevin, Division Science, 71 rue des Martyrs, 38042 Grenoble, France.

[3]CEA, Institut Nanosciences et Cryogénie, 17 rue des Martyrs, 38054 Grenoble, France.

[4]CEA, DRT, LITEN, Laboratoire de Nanocaractérisation et Nanosécurité, 17 rue des Martyrs, 38054 Grenoble, France.

[5]HZDR, ROBL beam line, European Synchrotron Radiation Facility, 71 rue des Martyrs, 38000 Grenoble, France

[6]Université Nice Sophia Antipolis, Institut de Chimie de Nice, UMR7272, 06108 Nice, France.

*Corresponding author: CEA, Laboratoire de Physiologie Cellulaire Végétale, 17 rue des Martyrs, 38054 Grenoble, France. Tel: +33 438789666. Fax: +33 438785091. Email: corinne.rivasseau@cea.fr

ABSTRACT

Microalgae are good candidates for toxic metal remediation biotechnologies. This study explores the cellular processes implemented by the green microalga *Coccomyxa actinabiotis* to take up and cope with silver over the concentration range 10^{-7} to 10^{-2} M Ag^{+}. Understanding these processes enables to assess the potential of this microalga in view to applications for bioremediation. Silver *in situ* speciation and localization were investigated using X-ray Absorption Spectroscopy, X-Ray diffraction and transmission electron microscopy. Silver toxicity was evaluated by monitoring microalgal growth and photochemical parameters. Different accumulation mechanisms were brought out depending on silver concentration. At low micromolar concentration, microalgae fixed all silver initially present in solution, trapping it inside the cells into the cytosol, mainly as unreduced Ag(I) bound with molecules containing sulfur. Silver was efficiently detoxified. When concentration increased, silver spread throughout the cell, particularly entering the chloroplast where it damaged the photosystem. Most silver was reduced to Ag(0) and aggregated to form crystalline silver nanoparticles of face-centered cubic structure, with a mean size of 10 nm. Additional minor interaction of silver with molecules containing sulfur indicated the concomitant existence of the mechanism observed at low concentration and/or nanoparticle capping. Nanoparticles were observed in chloroplasts, in mitochondria, on the plasma membrane, on cytosolic membrane structures and in vacuoles. Above 10^{-4} M Ag^{+}, damages were irreversible and cell died. However, high silver amounts remained confined inside microalgae, showing their potential for the bioremediation of contaminated water.

KEYWORDS. Silver, microalgae, speciation, reduction, nanoparticles, synchrotron X-ray absorption spectroscopy, EXAFS, XANES, X-ray diffraction, electronic microscopy.

INTRODUCTION

Contamination of the environment by heavy metals and radionuclides is a world concern which evolves with changing human uses. Among these contaminants, silver constitutes one of the most toxic metals in aquatic environments, at the same level as cadmium and chromium, surpassed only by mercury.[1] Silver toxicity depends on its speciation, the free cationic form Ag^+ being highly toxic.[1,2] Silver has long been used in the photographic and imaging industry, in the electrical and electronics industry, in jewelry, in the manufacture of silverware and coinage[3,4] as well as for the treatment of diseases and infections.[5] Recently, applications of its antimicrobial properties strongly developed, silver being now embedded in consumer products such as plasters, textiles, food containers, toothpaste or air filters in the form of nanoparticles and colloids.[6] Traditionally, silver is discharged into the environment from e.g. mining and industrial applications[4]. But it is also discharged nowadays from the normal use of consumer products which release silver nanoparticles, colloids and Ag^+.[7,8] Additionally, silver also constitutes one of the main gamma emitting radioactive contaminants present in liquid effluents issuing from nuclear pressurized water reactors operating in normal conditions, representing up to 48% of the gamma emitting radionuclides released.[9]

Remediation of effluents and of environmental water contaminated by heavy metals and radionuclides is currently mostly performed using conventional physico-chemical methods such as precipitation, oxidation/reduction or adsorption on ion-exchange resins. These methods suffer from several drawbacks including cost, intolerance to organic species, little efficiency for the removal of very low contaminant concentration and generation of large secondary waste volumes.[10] Biological remediation technologies based on organisms such as bacteria, fungi and plants have offered competitive alternatives in various fields. They

generally present a high efficiency, a wider field of application and lower cost and impact on the environment than physico-chemical technologies.[11,12] Microalgae are good candidates for heavy metal and radionuclide bioremediation strategies owing to their ability to fix a wide range of contaminants and to resist to their chemical toxicity thanks to their large surface-to-volume ratio, the structure of their cell wall carrying functional groups able to bind and immobilize contaminants and various mechanisms enabling metal incorporation and subcellular sequestration, excretion, or detoxification by speciation changes.[13] Algae-based biotechnologies for pollution remediation employ common green algae such as *Chlorella*, *Scenedesmus*, *Cladophora*, cyanobacteria or consortia of both.[14] Best metal accumulation performance is obtained with microalgal species isolated from long-term metal contaminated sites.[13] Recently, a unicellular green microalga, *Coccomyxa actinabiotis*, was isolated from an extreme environment contaminated with radioactive silver.[15] High fixation capacities were demonstrated for non-radioactive silver, namely 20 mg Ag g^{-1} fresh weight (FW), *i.e.* about 200 mg Ag g^{-1} dry weight (DW), among the higher values reported for various organisms. When exposed to high Ag^+ concentrations, up to 10^{-2} M, most silver accumulated inside the cell rather than on the mucilage surrounding the cell and the cell wall and formed silver aggregates.[16] *C. actinabiotis* showing also an extreme radiotolerance[15], it is therefore an ideal candidate in view to remove stable and radioactive silver both for remediation of contaminated environmental water and for its recovery from industrial effluents.

The present study aims at exploring some of the molecular and cellular mechanisms of silver accumulation and toxicity in *C. actinabiotis* in order to establish the potential of this promising microalga for bioremediation. The fundamental understanding of the mechanisms of silver uptake and toxicity constitutes the essential prerequisite for any biotechnological applications. As a result, key parameters can be controlled and optimized. Silver speciation was investigated directly *in situ* in microalgae suspended in Ag^+ solutions ranging from µM to

mM concentrations. As mentioned above, metals in excess relative to the cellular metabolic needs must be stored and/or their speciation modified to make them less toxic or facilitate their transport. Reduction processes, chelation by specific peptides or proteins such as ferritin, metallothioneins and phytochelatins or by small molecules may be involved.[17,18] A variety of analytical or spectroscopic methods have been used to study the speciation of metals in biological and environmental media, such as UV-visible, infrared, Raman, X-ray Absorption Spectroscopy (XAS), laser spectroscopy, mass spectrometry, nuclear magnetic resonance or separation techniques followed by elemental analysis.[19,20] XAS, comprising X-ray Absorption Near-Edge Structure (XANES) and Extended X-ray Absorption Fine Structure (EXAFS) spectra depending on the energy range above threshold, probes the near chemical environment of the central cation within 4-5 Å, with a sensitivity of up to tens of ppm. Technological advances made XAS suitable to study the speciation of metals also *in situ* in living organisms.[21] In this work, XAS (XANES and EXAFS), complemented by X-Ray diffraction (XRD), were used to investigate the silver speciation in *C. actinabiotis*, highlighting various oxidation states, coordination, and structure depending on the silver concentration. The progressive formation and localization of silver nanoparticles was investigated at different silver concentrations using electron microscopy (TEM), thus supplementing previous localization work.[16] Toxic effects of such Ag^+ concentrations to *C. actinabiotis* were then evaluated by monitoring physiological and biochemical parameters such as microalgal growth and photosynthetic capacity which are commonly used to assess metal toxicity to microalgae[22-24]. The combination of physiological, spectroscopic and physico-chemical investigations using techniques such as XAS, XRD, and TEM revealed the implementation of different cellular processes in the microalgae depending on silver concentration. Considerations about the remediation capabilities in view to use *C. actinabiotis* for the clean-up of contaminated water are presented.

101

102

MATERIALS AND METHODS

Algae culture. The microalga *Coccomyxa actinabiotis* used in this study is described previously.[15] Algal biomass was grown in batch mode in 800 mL round-bottom flasks aerated on an orbital shaker (Innova 2300, New Brunswick Scientific, Enfield, CT) at 100 rpm, under a continuous illumination of 70 $\mu E.m^{-2}.s^{-1}$, at 21 ± 2°C, in a modified Bold Basal Medium (BBM) culture solution (Sigma-Aldrich, Saint-Louis, MO) diluted twice with deionized water, and regularly sub-cultured to maintain cell growth.

Microalgae were harvested in the growing phase by centrifugation (2000 *g*, 5 min, 4°C), washed by three successive re-suspensions in deionized water followed by centrifugations (same conditions) to remove external elements coming from the culture medium, and finally re-suspended in ultrapure water (MilliQ, Millipore) at 2 $g_{FW}.L^{-1}$ to perform the experiments. Algae were exposed to silver nitrate ($AgNO_3$ Carl Roth GmbH, Karlsruhe, Germany) in ultrapure water rather than in culture medium in order to control silver speciation, which was the free form Ag^+ in all experiments. The microalga *C. actinabiotis* is known to grow naturally in ultra-pure water[15] where it was discovered, so that this medium change hardly affects its metabolism during the silver exposure protocol. Particularly, the photochemical parameter F_v/F_m of control algae varied by less than 10% over the time laps of exposure in pure water (Supplementary Figure S1A).

X-ray Absorption Spectroscopy

Sample preparation. The speciation of silver accumulated by microalgae was studied *in situ* using XAS. Microalgae were exposed to 10^{-6} M, 10^{-5} M and 10^{-4} M Ag^+ for 16 h, and to 10^{-3} M Ag^+ for 5 h, in polyethylene terephthalate glycol-modified (PETG) flasks, and incubated in the light, temperature, and aeration conditions listed above. After exposure, algae were

harvested by centrifugation and washed three times with water (2000 *g*, 5 min, 4°C). Silver concentration was determined in aliquots of pellet and supernatant by ICP-MS as described below. Pellets, in the form of a thick paste, were placed in polypropylene sample holders, sealed with Kapton®, plunged into liquid nitrogen, and kept at -80°C until analysis.

XAS measurements. Silver K-edge XANES and EXAFS spectra were collected at the Rossendorf Beamline at the European Synchrotron Radiation Facility (ESRF, Grenoble, France).[25] The beamline was equipped with a Si(111) double crystal monochromator, operated in channel-cut mode, and calibrated at the Ag K-edge energy of a Ag metal foil. Two Pt-coated Si mirrors were used to collimate the X-ray beam and achieve third-order harmonics rejection. Spectra were collected at 15 K using a ^{4}He cryostat. Samples were measured in fluorescence mode using a 13-element high purity Ge detector (Canberra) and in transmission mode using ionization chambers.

XAS analysis. XANES spectra were calibrated in energy using the Ag foil at 25514 eV (first point in the derivative) and normalized using the Athena code.[26] Silver form in the samples was qualitatively assessed by phenomenological comparison with reference spectra, namely Ag foil for Ag(0) metallic silver and Ag_2S for Ag-S bonding with formal oxidation state Ag(I). EXAFS data treatment was performed using the Athena code after background subtraction and normalization with Ifeffit routine, and then fitted using the Artemis code.[26] The EXAFS curves were extracted and k^2-weighted (k = wavenumber in $Å^{-1}$) for Fourier transformation between ca. 2.5 and 12 $Å^{-1}$. The fitting procedure was performed in real R space between 1 and 6 Å. Phases and amplitudes were calculated using Feff84 code[27]. For all Ag-Ag contributions, face-centered cubic (fcc) metallic silver was used as a model compound (crystallographic

153 data from Kittel[28]). 7 scattering paths corresponding to a cluster of 5.8 Å were selected
154 for the adjustment procedure: at 2.89 Å (2 legs), 4.09 Å (2 legs), 5.00 Å (2 legs), 5.39
155 Å (3 legs), and 5.78 Å (2, 3 and 4 legs). According to the fcc structure, all the paths were
156 linked together in the fitting procedure, so that only one Ag-Ag distance and one coordination
157 number were refined. When Ag-S contribution was also needed in the fit, it was
158 calculated using the structure of Ag_2S (crystallographic data from Frueh[29]). The spectra
159 of samples exposed to low silver concentrations were best fitted using a combination
160 of Ag-S and Ag-Ag single shell contributions; whereas the spectra of samples exposed
161 to the higher silver concentrations were fitted with the previously specified seven Ag-
162 Ag contributions together with an additional Ag-S single shell contribution.
163
164 **X-ray diffraction.** Silver speciation at high concentration was complemented by XRD
165 measurements. Algae were exposed to 10^{-2} M Ag^+, in PETG flasks, for 3 h, in the light or in
166 the dark, in the conditions described above. After exposure, algae were harvested by
167 centrifugation and washed twice with water (2000 *g*, 5 min, 4°C). Pellets were frozen in liquid
168 nitrogen and kept at -80°C. Right before analysis, samples were freeze-dried and ground into
169 a fine powder. A drop of water was added. The obtained paste was homogeneously spread on
170 zero-background silicon sample holders, allowed to dry, and covered with a Kapton® film. A
171 control sample (algae not exposed to silver) was prepared in the same conditions to measure
172 the algal baseline. Measurements were performed in Bragg-Brentano geometry, on a
173 PANalytical X'Pert diffractometer equipped with an X'Celerator linear detector, at $\lambda = 1.54$ Å
174 (Cu K_α emission lines). International Centre for Diffraction Data (ICDD) database
175 (http://www.icdd.com) was used to identify peaks; datasheet 00-004-0783 was used as
176 reference for fcc silver. To determine the crystallite size, the three most intense peaks were
177 fitted assuming a pseudo-Voigt shape function. A Scherrer type analysis[30] was performed

178 considering the resulting full widths at half maximum corrected from the instrumental
179 resolution.
180
181 **Transmission electron microscopy.** Silver localization in microalgae exposed to 10^{-4} M and 10^{-2} M Ag^{+} was analyzed using TEM as described in Leonardo *et al.* 2014.[16] To
183 determine the nanoparticle size distribution, the size of all particles in a given subcellular
184 compartment or in a given section of a compartment was measured.
185
186 **Inductively-coupled plasma-mass spectrometry**. Silver uptake was assessed directly
187 from silver concentration in microalgae using an inductively-coupled plasma-mass
188 spectrometry (ICP-MS) apparatus described previously[31] at m/z = 107 and 109, using
189 calibration solutions in 1% HNO_3 (v/v). Prior to ICP-MS analysis, algae pellets were
190 mineralized by suspension in 5 mL of concentrated HNO_3/HCl (2/1 v/v) (Suprapur® HNO_3
191 and HCl, Merck, Darmstadt, Germany) for 3 h at 170°C before dilution to 1% HNO_3 (v/v).
192
193 **Silver toxicity assessment.** Silver toxicity was assessed by monitoring the maximum
194 quantum yield of photosystem II F_v/F_m[24] and the cellular growth during silver exposure and
195 recovery. After exposure for 2 h to 10^{-7} M to 10^{-3} M Ag^{+} in the conditions described above, in
196 the light, microalgae were harvested by centrifugation, washed twice with water (2000 *g*,
197 5 min, 4°C) and allowed to recover in the culture conditions described above.
198
199
200

RESULTS AND DISCUSSION

In order to get insight into the mechanisms involved in silver accumulation, the *in situ* speciation of silver accumulated by *C. actinabiotis* was investigated. Algae exposed to 10^{-6} M, 10^{-5} M, 10^{-4} M, and 10^{-3} M Ag^+ accumulated respectively 51, 520, 2500, and 6500 $\mu g_{Ag}.g_{FW}^{-1}$, and were analyzed using XAS at the silver K edge. Two trends clearly appear for silver oxidation state and chemical environment depending on whether microalgae are exposed to low or high silver concentration.

The XANES spectra of algae samples were compared to the reference spectra of silver foil (Ag(0)) and Ag_2S in Figure 1. The XANES of the sample exposed to 10^{-6} M and 10^{-5} M Ag^+ are similar and display two weak oscillations separated by a plateau at ca. 25.52 and 25.54 keV. On the contrary, the samples exposed to 10^{-4} M and 10^{-3} M Ag^+ display two distinct oscillations at ca. 25.52 and 25.55 keV. From a qualitative comparison and despite the poor spectral resolution at this edge (about 6 eV from the core hole at this edge), it appears that the first set of spectra resembles that of the Ag_2S reference, whereas the second set is similar to the Ag foil reference. One may therefore assume that the environment of silver accumulated by the algae at low concentrations is comparable to that in Ag_2S whereas it is mostly reduced to Ag(0) at higher concentrations.

The EXAFS spectra are presented in Figure 2A and their corresponding Fourier transforms in Figure 2B, together with the fitted curves. As observed with the above XANES data, EXAFS spectra of the samples exposed to 10^{-4} M and 10^{-3} M Ag^+ are very similar. They exhibit clear oscillations up to 14 $Å^{-1}$. The high frequency of those oscillations and their shape suggests the presence of heavy backscattering atoms like Ag. In contrast, the spectra of algae exposed to 10^{-5} M and 10^{-6} M Ag^+ are different from the previous set. Despite the EXAFS spectrum of the latter being very noisy (and considered up to only 8 $Å^{-1}$) due to low silver

concentration in the sample, both spectra show oscillations which are in phase and have comparable amplitudes.

At low silver concentration (10^{-5} M), the Fourier transform of the EXAFS spectra exhibit two main contributions, at pseudo-distances of R + Φ = 1.9 Å and 2.75 Å. The spectra were successfully fitted (R factor = 3%) using two independent shells of Ag-S and Ag-Ag. Ag-O and Ag-N contributions were also tested and were ruled out because the corresponding distances were aberrant. These contributions correspond respectively to 2.0(1) S atoms located at an average distance of 2.41(1) Å and 0.9(1) Ag atoms located at 2.93(1) Å (Table 1). These fitted parameters are in good agreement with typical values reported in the literature for *in vitro* systems implying Ag and sulfur containing ligands. Silver EXAFS spectrum of Cd_2Ag_{17}-metallothioneins complexes has been for instance reported to be successfully fitted using 2 S atoms at 2.40 Å and an Ag contribution (without any indication of the coordination number) at 2.9 Å.[32] Ag-S average distances of 2.40(2) Å were also observed in Ag(+I)-penicillamine solutions.[33] Our results also indicate the presence of both two S in the first Ag coordination shell and one Ag neighbor. Sulfur neighbors are expected in ligands such as phytochelatins or metallothioneins. Nonetheless, the presence of an Ag neighbor in the structure is surprising and would indicate the occurrence of at least Ag dimers in the structure. Another assumption to explain this presence would be the concomitant formation of Ag nanoparticles (see below), although in very minor proportion, that would intermix with the presence of the sulfur compound. In any case these results suggest that Ag^+ ions accumulated by *C. actinabiotis* when exposed to low concentrations react with cellular molecules and complex to sulfur containing groups. This is consistent with the preferential chemical interaction between silver(I) ions and thiol-containing species.[34,35] Free Ag^+ ions are complexed by thiol-containing species such as cysteine, glutathione, metallothioneins or phytochelatins known to be involved in metal detoxification mechanisms. *In vivo*, silver has

been shown to bind both high-molecular-weight substances and metallothioneins in the hepatocytosol of animals[36] and to induce phytochelatin synthesis in microalgae[37]. In the context of bioremediation, the change in silver speciation enables the immobilization of the metallic ion inside the *C. actinabiotis* cells in a non-toxic form and preserves the cellular functioning as will be shown by the toxicity experiments presented below. This is the main phenomenon occurring at silver concentrations representative of that contained in industrial effluents which are of the order of 10^{-6}-10^{-5} M.

At higher silver concentrations (10^{-4} M and 10^{-3} M), we observed from the EXAFS, XRD, and TEM results the formation of silver metal nanoclusters inside the algae cells themselves. The EXAFS spectra were strongly dominated by Ag-Ag backscattering, which accounted for the contributions at pseudo-distances of $R + \Phi = 2.7$, 3.9, 4.9, and 5.5 Å on the Fourier transform (Figure 2B). All these peaks were successfully fitted using the fcc silver model described in the experimental section. The first Ag-Ag distances are equal to 2.87(2) and 2.87(1) Å and average coordination numbers equal to 3.6(1) and 3.9(1) for samples exposed to 10^{-4} M and 10^{-3} M, respectively. These distances are remarkably consistent with an Ag(0) fcc phase as described in the experimental section (list of all the paths in Table S1 of the Supporting Information). It is also in agreement with distances reported for silver nanoclusters embedded in glass (2.88(1) Å at 15 K)[38] or synthesized by living alfalfa sprouts (2.88 Å).[39] The low value of the Ag-Ag coordination numbers (respectively 3.6(1) and 3.9(1)) compared to the fcc structure (coordination number equals to 12) suggests a deviation from a pure fcc phase and the presence of silver nanoclusters within the algae, as observed previously using TEM.[16] It is actually known that small metal clusters have smaller average coordination numbers than bulk structures because the atoms located at the surface of the cluster have less neighboring atoms, which causes the decrease of the average coordination number. Montejano-Carrizales and co-workers reported a formula that links the average

coordination number of a cluster to its diameter, assuming the cluster is rather small (10-1000 atoms) and spherical.[40] When applying this formula to the present results, an fcc silver cluster with an average coordination number of about 4 corresponds to a particle diameter of the order of few nms. However one might keep in mind that an average coordination number of 4 may also be obtained when numerous small clusters of a few silver atoms or even isolated atoms are present together with some large clusters of few tens of nm. Such low Ag-Ag coordination number has already been observed in the case of Ag nanoparticles embedded in a silica glass and attributed to the presence of Ag-O contributions.[41]

Indeed, beside the strong Ag-Ag interactions, the Fourier transform of the EXAFS spectra of samples exposed to high silver concentrations exhibit a zone of disagreement at a pseudo-distance of ca. $R + \Phi = 2$ Å. Although this zone is strongly affected by the lobes of the Fourier transform of the Ag-Ag scattering, we attempted to fit this zone with an additional low R contribution. At first the presence of O neighbors has been tested and gave a satisfactory agreement in this zone. This corresponds to a distance of ca. 2.20 Å. Several oxygenated biological ligands have actually been shown to bind silver.[34] Dubiel and co-workers fitted similar spectra with Ag-O contributions at 2.13-2.14 Å when studying silver speciation in silicate glasses.[41] However, the longer distance obtained in our study makes the hypothesis of O neighbors as a first shell unlikely. Instead this contribution may be fitted using an additional Ag-S shell that significantly improved the fit (R factor from 0.039 to 0.019). It corresponds to 0.7(1) S at a distance of 2.46(1) Å. This bond length is in agreement with values reported for silver bound to rabbit liver metallothioneins MT1 (2.45(2) and 2.44(3) Å for Ag_{12}-MT1 and Ag_{17}-MT1, respectively).[42] It is also comparable with the Ag-S distance determined for silver concentration equal to 10^{-5} M. However the very low coordination number suggests considering this additional contribution with care because the

300 interference between a minority of Ag-S and a majority of Ag-Ag backscatters at such low R
301 distance value is strongly influenced by the amplitude of the latter.

302 Given the above data, it can be assumed that the reduced silver nanoparticles described
303 above coexist with unreduced isolated silver species (silver ions bound to thiols for instance)
304 as observed for the lowest concentrations. In addition, part of the surface atoms of the
305 nanoparticles may be linked to sulfur atoms (or much less likely to oxygen atoms) capping
306 and stabilizing the nanoparticles. This suggests that the algae accumulate Ag(+I) sulfur
307 species (like at low silver concentrations) but reduce Ag^+ into Ag(0) nanoparticles when the
308 silver exposure increases. It is likely that these different mechanisms coexist.
309
310 The crystallinity of the silver nanoparticles formed inside algae was further
311 investigated using X-Ray diffraction after freeze-drying. The diffractogram of control algae
312 exposed to no silver showed that the spectra baseline is distorted because of the amorphous
313 phases present in the freeze-dried algae and of the kapton® film. The diffractogram of algae
314 exposed to 10^{-2} M Ag^+ displays noticeable peaks at $2\theta = 38.1°$, 44.3°, 64.4°, and 77.5° (Figure
315 3), corresponding to the fcc silver reference diffraction pattern (planes (111), (200), (220), and
316 (311), respectively), which clearly indicates the existence of fcc silver nanoparticles inside the
317 algae. Silver crystals probably form independently from any light processes as they appeared
318 in microalgae exposed to Ag^+ in the light as well as in the dark (Figure 3). The three most
319 intense peaks (111), (220), and (311) obtained on the diffractogram were fitted assuming a
320 pseudo-Voigt shape function. A Scherrer type analysis lead to a mean crystallite size of 10 ± 2
321 nm. But the peak shape indicates the presence of a broad distribution. These results are
322 consistent with previous TEM observation of similar samples which highlighted the presence
323 of clusters containing silver as revealed by energy dispersive spectroscopy analysis[16], and
324 whose size ranged from some nm to about 30 nm.[16] This is compatible also with the EXAFS

data at 10^{-4} M and 10^{-3} M. It demonstrates the fcc structure of *in situ* synthesized silver nanoparticles by *Coccomyxa actinabiotis*. The synthesis of silver nanoparticles by dead or living biomass, including plant extracts[43,44], plants[39], bacteria[45] and recently the green microalga *Chlamydomonas reinhardtii*[46], has been reported. However, the crystallinity of these particles had not been assessed in microalgae. When crystallinity was assessed, plant extract were shown to yield two kinds of silver crystal structures, namely hexagonal and fcc[47]. The fcc crystals obtained here in *Coccomyxa actinabiotis* are thermodynamically the most stable configuration compared to hexagonal structures which are metastable.[48,49]

Nanoparticles localization and size were examined using TEM in microalgae exposed to 10^{-4} M and 10^{-2} M Ag^{+}. At 10^{-4} M, nanoparticles appear mainly in the chloroplast and in mitochondria (Figure 4A,B). The distribution of particle size is monodisperse, ranging from 4 to 28 nm, with most particles in the 6 to 12 nm range (Supplementary Figure S2A). The presence of even smaller particles cannot be excluded but is difficult to infer from the images. The biggest clusters may correspond to agglomerates of smaller nanoparticles. The plastid localization agrees with Beattie and co-workers observations on living plants showing that silver nanoparticles are most abundant in the chloroplasts of *Brassica juncea* exposed to 2 10^{-2} M Ag^{+}.[50] However, in *Chamydomonas reinhardtii* exposed to 10^{-3} M Ag^{+}, nanoparticles are localized in the peripheral cytoplasm and at flagella root.[46] The discrepancy between both green microalgae may be due to different stages of nanoparticles formation related to different response thresholds to silver.

When silver intracellular concentration increases, silver nanoparticles appear in almost all cellular compartments, namely in the chloroplast, in mitochondria, in the cytosol along the plasma membrane, on membrane structures such as Golgi apparatus and in vacuoles (Figure 4C,D). This localization is consistent with previous observations using nano X-ray

fluorescence.[16] The distribution of particle size is comparable to that observed at lower silver concentrations, with most particles in the 6 to 12 nm range (Supplementary S2A) and is identical whatever the subcellular cell compartment, whether being the chloroplast, mitochondria or vacuoles (Supplementary Figure S2B). This distribution is consistent with the mean particle size of 10 nm evaluated by X-ray diffraction in algae exposed to 10^{-2} M Ag. The somewhat higher size of some clusters may result from the aggregation of crystallites or coalescence of smaller nanoparticles as observed in Figure 4D and reported by Gardea-Torresdey and co-workers.[39]

The formation of silver nanoparticles actually implies the reduction of Ag^+ and the nucleation of the metallic seeds, their growth with the aggregation of these small nuclei and their stabilization by capping molecules[51] like oxygen, nitrogen, or sulfur containing molecules. In microalgae, their formation probably relies on different simultaneous mechanisms, several molecules being able to be implied in Ag^+ reduction and nanoparticles stabilization. Various enzymes such as ATP synthase, superoxide dismutase, carbonic anhydrase and ferredoxin-$NADP^+$ reductase have been shown to be associated with *in vivo* synthesis of silver nanoparticles in *Chamydomonas reinhardtii*.[46] Plant extracts containing aldehyde, amino and carboxyl functions[44,52] as well as the chemical species oxygen superoxide O_2^- [53] have also been demonstrated to synthesize silver or gold nanoparticles or assist their synthesis. Moreover, owing to the high reducing potential of Ag^+ of 0.8V, many reducing metabolites such as NADH, NADPH, glutathione or ferredoxin, whose respective redox potential are about -0.32V, -0.32V, -0.22V, and -0.43V [54], are thermodynamically able to reduce Ag^+. The initial localization of silver nanoparticles of substantial size in the chloroplast and mitochondria may result from several favorable dispositions. First, these compartments contain high amounts of adequate reducing metabolites such as ferredoxin and

NADPH in plastids and NADH, $FADH_2$, $FMNH_2$ in mitochondria. Secondly, the chloroplast contains enzymes shown to be associated with nanoparticle formation as mentioned above, such as ferredoxin-$NADP^+$ reductase, carbonic anhydrase, superoxide dismutase, and ATP synthase, the latter two being also present in mitochondria. It is noteworthy that nanoparticles seem to form in intermembrane mitochondrial space rather than in mitochondrial matrix (Figure 4). A high local free Ag^+ concentration, together with favorable reduction and nucleation conditions, probably favors the formation of particles of substantial size in intermembrane space, whereas their formation in matrix is probably hampered by the low free Ag^+ concentration owing to the very high metabolite and protein density, in the order of 400 $mg.mL^{-1}$,[55] or to limited Ag^+ passing through the membrane. Nanoparticle smaller size in microalgae compared to that obtained in different *ex vivo* conditions[47,56] may be related to growth limitation owing to local Ag^+ depletion as well as to capping by various soluble or membrane molecules.

The toxic effects of such silver concentrations to *C. actinabiotis* were examined. Silver toxicity was assessed both during and after exposure by monitoring algal growth and photosynthetic capacity. Growth actually reflects the overall physiological state of the cell including various fundamental physiological and biochemical processes, and the photosynthetic activity is the basis for cell development in these autotrophically-grown algae. Photosynthetic capacity was assessed through the measurement of the chlorophyll-a fluorescence yield F_v/F_m.[24] This parameter is very sensitive to metal toxicity.[23,57] As for silver speciation and subcellular localization, two different behaviours were brought out, depending on whether *C. actinabiotis* was exposed to low ($\leq 10^{-5}$ M) or high ($\geq 10^{-4}$ M) silver concentration (Supplementary Figure S1). During exposure to silver, the photochemical yield of microalgae contacted with low micromolar Ag^+ concentrations did not change. An about

two fold reduction was noticed at 10^{-5} M but the microalgae recovered their photosynthetic capacities within about four days when transferred into a silver-free growth medium (Supplementary Figure S1A). Contrastingly, the photochemical yield of microalgae contacted with higher Ag^+ concentrations quickly dropped to zero, within 2 h, indicating that the photosynthetic apparatus was strongly damaged (Supplementary Figure S1A). The decrease in the F_v/F_m yield may result from Ag^+ substitution to Cu^+ in photosynthetic metalloproteins, both elements possessing close chemical reactivity. It was actually shown that the replacement of Cu^+ by Ag^+ in plastocyanine and cytochrome complex resulted in the inactivation of the photosynthetic electron transport.[58] The ability of *C. actinabiotis* to recover from silver exposure was further tested by transferring the microalgae into a silver-free culture medium. Low micromolar silver concentrations did not affect growth as compared to control (Supplementary Figure S1B). At the turning point of 10^{-5} M, cells were able to actively detoxify silver and returned to a growth identical to that of control algae after a recovery period of about four days. Conversely, the photosynthetic apparatus in microalgae exposed to higher silver concentrations was irreversibly damaged. Their photochemical yield and their growth rate remained at zero (Supplementary Figures S1A and S1B). The photosynthesis inhibition could be sufficient to prevent cell growth; however, other processes may also be affected. The half maximum effective concentration (EC_{50}) of Ag^+ toxicity in these conditions was therefore of the order of 10 µM, which is above toxicity values reported for other green microalga, though experimental conditions were different. EC_{50} of about 10-20 nM and 25 nM have actually been reported for growth inhibition of *Chlamydomonas reinhardtii* and *Pseudokirchneriella subcapitata*, respectively,[59,60] and about 200 nM for the inhibition of the photosynthetic yield in *Chlamydomonas reinhardtii*.[61] The somewhat higher resistance of *C. actinabiotis* to silver toxicity makes it of interest for remediation processes based on a living biomass.

In conclusion, this work highlights the progressive change in processes implemented by *Coccomyxa actinabiotis* to take up and cope with silver when exposed to increasing Ag^+ concentration. The simultaneous monitoring of silver *in situ* speciation and localization in relation to toxicity brought out two mechanisms, one prevailing at low micromolar Ag^+ concentration, the other at high concentration, above 10^{-4} M Ag^+. They are reported here together in living algae and plants for the first time, to the best of our knowledge. At low micromolar concentration, microalgae take up and sequester all silver initially present in solution, thus totally purifying the water. Silver is internalized in the cell and trapped in the cytosol[16] mainly as unreduced Ag(+I) bound by sulfur containing molecules. It is likely that this chelation is the first mechanism that stops Ag^+ diffusion inside the cell. This is probably part of an efficient detoxification process as the microalgal growth and photosynthetic activity actually remained unaffected. In the context of bioremediation, the knowledge of this mechanism provides the necessary information to optimize the sequestration capacities. This could be performed by genetic engineering to enhance the synthesis of these key metabolites and by providing the microalgae with adequate sulfate amounts. When silver external concentration increases, the stronger Ag^+ intracellular influx overwhelms the sulfur complexation mechanisms. They prove insufficient to stop Ag^+ in the cytosol and overcome its toxicity. Silver spreads throughout the cell. Most silver is reduced to Ag(0) and aggregates to form crystalline silver nanoparticles of about 10 nm, with a fcc structure. At 10^{-4} M Ag^+, nanoparticles appear particularly in the chloroplast and mitochondria, organelles containing high reducing power and enzymes involved in oxidoreductive mechanisms. Nanoparticles formation may be one way to reduce silver toxicity once the complexation mechanisms by sulfur ligands are overwhelmed, as silver nanoparticles are less toxic than free Ag^+.[62] But even if it were the case, this process reveals insufficient or not quick enough to protect the

450 photosynthetic apparatus (the photochemical parameters collapsed when silver reaches the
451 chloroplast) and prevent lethal effect beyond 10^{-4} M Ag^{+}. When silver concentration still
452 increases, nanoparticles continue to form, despite cell death, as observed with biomass
453 extracts[44,52] and the amount of silver accumulated by microalgae continues to increase.
454 Besides, interactions of silver with S still occur at high Ag^{+} concentration. Molecular
455 mechanisms of Ag^{+} complexation and nanoparticles formation need further investigation.
456 Nonetheless, even at 10^{-2} M Ag^{+}, nanoparticles remain trapped inside microalgae, mostly
457 embedded in intracellular membranes structures, which constitutes an asset for the
458 bioremediation of contaminated effluents and environmental water. It is noteworthy that
459 whatever the cellular mechanisms implemented (molecular chelation by sulfur groups or
460 cluster formation), silver remains confined inside the cells.

461 The usual metal concentration limit in effluents issuing from the mining industry is
462 around 1 $mg.L^{-1}$. In such conditions, the full silver load can be trapped into the algae. Our
463 results also imply that effluent containing higher silver concentrations could be processed
464 before being discharged into the environment, with similar remediation efficiency. Even
465 higher concentrations will lead to the formation of silver nanoclusters and eventually to the
466 algae cell death, but algae still constitute efficient bioremediators as nanoparticles will remain
467 within the cells.

468 Further work will involve the application to polluted water, from e.g. aqueous
469 effluents in the case of industrial applications, or fresh water stream in environmental
470 application, using a bioreactor developed at laboratory pilot scale for other applications of this
471 microalga[63]. After depollution of the effluent by an algal suspension, the microalgae could be
472 separated by micro-filtration or centrifugation. The fact that high amounts of silver are
473 sequestered inside algae is of relevance to bioremediation as well as to recycling technologies.
474 Recovery of silver from the collected algae could be considered as a new supply strategy.

475

476

477 **ACKNOWLEDGEMENTS**

478

479 The authors gratefully acknowledge the Transversal Nuclear Toxicology Program of the CEA
480 and the ILL for financial support, Annie Rivoire and Christelle Boulé for TEM analyses,
481 Mélanie Auffan for the silver sulfide XANES spectra, Olivier Proux for advice, and Richard
482 Bligny and Jacques Bourguignon for fruitful discussion. XAS experiments were carried out at
483 the ROBL beam line of ESRF, in Grenoble, France, and TEM analyses at the Centre
484 Technologique des Microstructures - Plateforme de l'Université Claude Bernard Lyon 1.

485

486

487 **ASSOCIATED CONTENT**

488

489 **Supporting Information Available**

490

491 Table S1. Best fit parameters from the refinement of the algae samples exposed to silver
492 EXAFS spectra with the list of all the Ag-Ag distances included in the fitting procedure of
493 algae samples exposed to silver at 10^{-3} and 10^{-4} M.
494 Figure S1. Physiological impact of silver on *C. actinabiotis* exposed to various Ag^{+}
495 concentrations and recovery thereafter including the changes in photosynthetic yield and algal
496 growth.
497 Figure S2. Size distribution of nanoparticles in microalgae.
498 This information is available free of charge via the Internet at http://pubs.acs.org.

499

500 **REFERENCES**

501

502 (1) Ratte, H. T. Bioaccumulation and toxicity of silver compounds: A Review. *Environ.*
503 *Toxicol. Chem.* **1999**, *18* (1), 89–108; DOI 10.1002/etc.5620180112.

504 (2) Stevenson, L. M.; Dickson, H.; Klanjscek T.; Keller, A. A.; McCauley, E.; Nisbet, R. M.
505 Environmental Feedbacks and Engineered Nanoparticles: Mitigation of Silver Nanoparticle
506 Toxicity to *Chlamydomonas reinhardtii* by Algal-Produced Organic Compounds. PLoS ONE
507 **2013**, *8* (9), e74456; DOI 10.1371.

508 (3) *World Silver Summary*; Thomson Reuters GFMS, 2013.

509 (4) Purcell, T. W.; Peters, J. J. Sources of silver in the environment. *Environ. Toxicol. Chem.*
510 **1998**, *17* (4), 539–546; DOI 10.1002/etc.5620170404.

511 (5) Rai, M.; Yadav, A.; Gade, A. Silver nanoparticles as a new generation of antimicrobials.
512 *Biotechnol. Adv.* **2009**, *27* (1), 76–83; DOI 10.1016/j.biotechadv.2008.09.002.

513 (6) Klaine, S. J.; Alvarez, P. J. J.; Batley, G. E.; Fernandes, T. F.; Handy, R. D.; Lyon, D. Y.;
514 Mahendra, S.; McLaughlin, M. J.; Lead, J. R. Nanomaterials in the environment: behavior,
515 fate, bioavailability, and effects. *Environ. Toxicol. Chem.* **2008**, *27* (9), 1825–1851.

516 (7) Benn, T. M.; Westerhoff, P. Nanoparticle silver released into water from commercially
517 available sock fabrics. *Environ. Sci. Technol.* **2008**, *42* (11), 4133–4139; DOI
518 10.1021/es7032718.

519 (8) Kaegi, R.; Sinnet, S.; Zuleeg, S.; Hagendorfer, H.; Mueller, E.; Vonbank, R.; Boller, M.;
520 Burkhardt, M. Release of silver nanoparticles from outdoor facades. *Environ. Pollut.* **2010**,
521 *158* (9), 2900–2905. DOI 10.1016/j.envpol.2010.06.009.

(9) Florence, D.; Hartmann, P. *Les rejets radioactifs et chimiques des centrales nucléaires d'EDF*. EDF/CAPE Saint-Denis, 2003.

(10) Eccles, H. Treatment of metal-contaminated wastes: why select a biological process? *TIBTECH* **1999**, *17*, 462–465.

(11) Gadd, G. M. Metals, minerals and microbes: geomicrobiology and bioremediation. *Microbiol.* **2010**, *156* (3), 609–643; DOI 10.1099/mic.0.037143-0.

(12) Gillespie, I. M. M.; Philp J. C. Bioremediation, an environmental remediation technology for the bioeconomy. *Trends Biotechnol.* **2013**, *31*, 329–332; DOI 10.1016/j.tibtech.2013.01.015.

(13) Monteiro, C. M.; Castro, P. M. L.; Malcata, F. X. Metal uptake by microalgae: underlying mechanisms and practical applications. *Biotechnol. Prog*. **2012**, *28* (2), 299–311; DOI 10.1002/btpr.1504.

(14) Perales-Vela, H. V.; Peña-Castro, J. M.; Cañizares-Villanueva, R. O. Heavy metal detoxification in eukaryotic microalgae. *Chemosphere* **2006**, *64* (1), 1–10; DOI 10.1016/j.chemosphere.2005.11.024.

(15) Rivasseau, C.; Farhi, E.; Atteia, A.; Couté, A.; Gromova, G.; de Gouvion Saint Cyr, D.. Boisson, A.-M.; Féret, A.-S.; Compagnon, E.; Bligny, R. An extremely radioresistant green eukaryote for radionuclide bio-decontamination in the nuclear industry. *Energy Environ. Sci.* **2013**, *6* (4), 1230–1239; DOI 10.1039/c2ee23129h.

(16) Leonardo, T.; Farhi, E.; Boisson, A.-M.; Vial, J.; Cloetens, P.; Bohic, S.; Rivasseau, C. Determination of elemental distribution in green micro-algae using synchrotron radiation nano X-ray fluorescence (SR-nXRF) and electron microscopy techniques – subcellular

544 localization and quantitative imaging of silver and cobalt uptake by Coccomyxa actinabiotis.
545 *Metallomics* **2014**, *6* (2), 316–329; DOI 10.1039/c3mt00281k.

546 (17) Clemens, S. Toxic metal accumulation, responses to exposure and mechanisms of
547 tolerance in plants. *Biochimie* **2006**, *88*, 1707–1719.

548 (18) Meharg, A. A. Mechanisms of plant resistance to metal and metalloid ions and potential
549 biotechnological applications. *Plant Soil* **2005**, *274*, 163–174.

550 (19) Lombi, E.; Scheckel, K. G.; Kempson, I. M. In situ analysis of metal(loid)s in plants:
551 State of the art and artefacts. *Environ. Exp. Bot.* **2011**, *72*, 3-17.

552 (20) Ménager, M.-T.; Garnier-Laplace, J.; Goyffon, M. Eds. *Toxicologie Nucléaire*
553 *Environnementale et Humaine*. Tec & Doc Lavoisier: Paris, 2009.

554 (21) Sarret, G.; Pilon Smits, E. A. H.; Castillo Michel, H.; Isaure, M. P.; Zhao, F. J.; Tappero,
555 R. Use of synchrotron-based techniques to elucidate metal uptake and metabolism in plants.
556 In *Advances in Agronomy*, Sparks, D.L. Ed.; Academic Press: San Diego, CA 2013; Vol. 119,
557 pp 1–82.

558 (22) Monteiro, C. M.; Castro, P. M. L.; Malcata, F. X. Metal Uptake by Microalgae:
559 Underlying Mechanisms and Practical Applications. Biotechnol. Prog., **2012**, *28*, 299–311.

560 (23) Cardol, P.; Bailleul, B.; Rappaport, F.; Derelle, E.; Béal, D.; Breyton, C.; Bailey, S.;
561 Wollman, F.-A.; Grossman, A. R.; Moreau, H.; Finazzi, G. 2008. An original adaptation of
562 photosynthesis in the marine green alga *Ostreococcus. Proc. Natl. Acad. Sci. U S A*. **2008**,
563 *105*, 7881–7886.

564 (24) Suresh, K. K.; Dahms, H.-U.; Lee, J.-S.; Kim, H. C.; Lee, W. C.; Shin., K.-H. Algal
565 photosynthetic responses to toxic metals and herbicides assessed by chlorophyll a
566 fluorescence " *Ecotoxicol. Environ. Safety*. **2014**, *104*, 1–71.

567 (25) Matz, W.; Schell, N.; Bernhard, G.; Prokert, F.; Reich, T.; Claußner, J.; Oehme, W.; et
568 al. ROBL – a CRG beamline for radiochemistry and materials research at the ESRF. *J.*
569 *Synchrotron Rad.* **1999**, *6* (6), 1076–1085; DOI 10.1107/S0909049599010663.

570 (26) Ravel, B.; Newville, M. ATHENA, ARTEMIS, HEPHAESTUS: data analysis for X-ray
571 absorption spectroscopy using IFEFFIT. *J. Synchrotron Rad.* **2005**, *12* (4), 537–541; DOI
572 10.1107/S0909049505012719.

573 (27) Rehr, J. J.; Albers, R. C. Theoretical approaches to x-ray absorption fine structure. *Rev.*
574 *Modern Phys.* **2000**, *72* (3), 621–654; DOI 10.1103/RevModPhys.72.621.

575 (28) Kittel, C. *Introduction to Solid State Physics*. Wiley Ed., New York, 2004.

576 (29) Frueh, A. J. The crystallography of silver sulfide, Ag_2S. *Z. Kristallogr.* **1958**, *110*, 136–
577 144.

578 (30) Scherrer P. Bestimmung der Größe und der inneren Struktur von Kolloidteilchen mittels
579 Röntgenstrahlen. *Göttinger Nachrichten Gesell.*, **1918**, *2*, 98.

580 (31) Rivasseau, C.; Seemann, M.; Boisson, A.-M.; Streb, P.; Gout, E.; Douce, R.; Rohmer,
581 M.; Bligny, R. Accumulation of 2-C-methyl-D-erythritol 2,4-cyclodiphosphate in illuminated
582 plant leaves at supraoptimal temperatures reveals a bottleneck of the prokaryotic
583 methylerythritol 4-phosphate pathway of isoprenoid biosynthesis. *Plant Cell Environ.* **2009**,
584 *32* (1), 82–92; DOI 10.1111/j.1365-3040.2008.01903.x.

(32) Hasnain, S. S.; Diakun, G. P.; Abrahams, I.; Ross, I.; Garner, C. D.; Bremner, I.; Vasak, M. EXAFS Studies of Metallothionein. *Experientia. Suppl.* **1987**, *52*, 227–236.

(33) Leung, B. O.; Jalilehvand, F.; Mah, V.; Parvez, M.; Wu,Q. Silver(I) complex formation with cysteine, penicillamine, and glutathione. *Inorg. Chem.* **2013**, *52* (8), 4593–4602; DOI 10.1021/ic400192c.

(34) Bovenkamp, G. L.; Zanzen, U.; Krishna, K. S.; Hormes, J.; Prange A. X-ray absorption near-edge structure (XANES) spectroscopy study of the interaction of silver ions with Staphylococcus aureus, Listeria monocytogenes, and Escherichia coli. *Appl. Environ. Microbiol.* **2013**, *79* (20): 6385–6390; DOI 10.1128/AEM.01688-13.

(35) Nieboer, E.; Richardson, D. H. S. The replacement of the nondescript term 'heavy metals' by a biologically and chemically significant classification of metal ions. *Environ. Pollut. Ser. B* **1980**, *1* (1), 3–26; DOI 10.1016/0143-148X(80)90017-8.

(36) Ikemoto, T.; Kunito, T.; Anan, Y.; Tanaka, H.; Baba, N.; Miyazaki, N.; Tanabe, S. Association of heavy metals with metallothionein and other proteins in hepatic cytosol of marine mammals and seabirds. *Environ. Toxicol. Chem.* **2004**, *23*, 2008–2016.

(37) Gekeler, W.; Grill, E.; Winnacker, E.-L.; Zenk, M. H. Algae sequester heavy metals via synthesis of phytochelatin complexes. *Arch. Microbiol*. **1988**, *150*, 197–202.

(38) Dubiel, M.; Yang, X. C.; Brunsch, S. Investigation of Stress State of Silver Nanoparticles in Silicate Glasses by Means of EXAFS. *Phys. Scripta* **2005**, 729; DOI 10.1238/Physica.Topical.115a00729.

(39) Gardea-Torresdey, J. L.; Gomez, E.; Peralta-Videa, J. R.; Parsons, J. G.; Troiani, H.; Jose-Yacaman, M. Alfalfa Sprouts: A natural source for the synthesis of silver nanoparticles. *Langmuir* **2003**, *19* (4), 1357–1361; DOI 10.1021/la020835i.

608 (40) Montejano-Carrizales, J. M.; Aguilera-Granja, F.; Morán-López, J. L. Direct
609 enumeration of the geomerical characteristics of clusters. *Nanostruc. Mater.* **1997**, *8* (3), 269–
610 287. DOI 10.1016/S0965-9773(97)00168-2.

611 (41) Dubiel, M.; Brunsch, S.; Tröger, L. Characterization of nanoscale silver particles in
612 glasses by temperature-dependent EXAFS spectroscopy. *J. Phys.: Condens. Matter* **2000**, *12*,
613 4775–4789.

614 (42) Gui, Z.; Green, A. R.; Kasrai, M.; Bancroft, G. M.; Stillman, M. J. Sulfur K-Edge
615 EXAFS Studies of Cadmium-, Zinc-, Copper-, and Silver-Rabbit Liver Metallothioneins.
616 *Inorg. Chem.* **1996**, *35* (22), 6520–6529; DOI 10.1021/ic951624m.

617 (43) Sanchez-Mendieta, V.; Vilchis-Nestor, A. R. Green synthesis of noble metals (Au, Ag,
618 Pt) nanoparticles assisted by plant-extracts. In *Noble Metals*; Su, Y.-H., Ed.; InTech: Rijeka,
619 Croatia. 2012; pp 391–408.

620 (44) Peng, H.; Yang, A.; Xiong, J. Green, microwave-assisted synthesis of silver
621 nanoparticles using bamboo hemicelluloses and glucose in an aqueous medium. *Carbohydr.*
622 *Polym.* **2013**, *91* (1), 348–355; DOI 10.1016/j.carbpol.2012.08.073.

623 (45) Kalimuthu, K.; Suresh Babu, R.; Venkataraman, D.; Bilal, M.; Gurunathan, S.
624 Biosynthesis of silver nanocrystals by Bacillus licheniformis. *Colloids Surf. B Biointerfaces*
625 **2008**, *65* (1), 150–153; DOI 10.1016/j.colsurfb.2008.02.018.

626 (46) Barwal, I.; Ranjan, P.; Kateriya S.; Yadav, S. C. Cellular oxido-reductive proteins of
627 Chlamydomonas reinhardtii control the biosynthesis of silver nanoparticles. *J.*
628 *Nanobiotechnology* **2011**, *9* (1), 1–12; DOI 10.1186/1477-3155-9-56.

629 (47) Rodríguez-León, E.; Iñiguez-Palomares, R.; Navarro, R. E.; Herrera-Urbina, R.;
630 Tánori,J.; Iñiguez-Palomares, C.; Maldonado, A. Synthesis of silver nanoparticles using

631 reducing agents obtained from natural sources (Rumex hymenosepalus extracts). *Nanoscale*
632 *Res. Lett.* **2013**, *8*, 318; DOI 10.1186/1556-276X-8-318.

633 (48) Jona, F.; Marcus, P. M. Metastable phases of silver and gold in hexagonal structure. *J.*
634 *Phys.: Condens. Matter* **2004**, *16*, 5199–5204.

635 (49) Novgorodova, M. I.; Gorshkov, A. I.; Mokhov, A. V. Native silver and its new structural
636 modifications. *Int. Geol. Rev.* **1981**, *23* (4), 485–494.

637 (50) Beattie, I. R.; Haverkamp, R. G. Silver and gold nanoparticles in plants: sites for the
638 reduction to metal. *Metallomics* **2011**, *3*, 628–632; DOI 10.1039/c1mt00044f.

639 (51) Lukman, A. I.; Gong, B.; Marjo, C. E.; Roessner, U.; Harris, A. T. Facile synthesis,
640 stabilization, and anti-bacterial performance of discrete Ag nanoparticles using Medicago
641 sativa seed exudates. *J. Colloid Interface Sci.* **2011**, *353*, 433–444.

642 (52) Gardea-Torresdey, J. L.; Tiemann, K. J.; Parsons, J. G.; Gamez, G.; Herrera, I.; Jose-
643 Yacaman, M. XAS investigations into the mechanism (s) of Au (III) binding and reduction by
644 alfalfa biomass. *Microchem. J.* **2002**, *71* (2), 193–204.

645 (53) Jones, A. M.; Garg, S.; He, D.; Pham, A.N.; Waite, T. D. Superoxide-mediated formation
646 and charging of silver nanoparticles. *Environ. Sci. Technol.* **2011**, *45* (4), 1428–34 ; DOI
647 10.1021/es103757c.

648 (54) Hopkins, W. G. *Physiologie Végétale*; Rambour, S. Trad.; De Boeck Ed., 2003.

649 (55) Douce, R. *Mitochondria in Higher Plants*; Academic Press Inc.; Orlando, Florida, 1985.

650 (56) Yoosaf K.; Ipe, B. I.; Suresh, C. H.; Thomas, K. G. In situ synthesis of metal
651 nanoparticles and selective naked-eye detection of lead ions from aqueous media. *J. Phys.*
652 *Chem. C.* **2007**, *111,* 12839–12847.

(57) Baumann, H. A.; Morrison, L.; Stenge, D. B. Metal accumulation and toxicity measured by PAM–Chlorophyll fluorescence in seven species of marine macroalgae. *Ecotoxicol. Environ. Safety*. **2009**, *72*, 1063–1075.

(58) Sujak A. Interaction between cadmium, zinc and silver-substituted plastocyanin and cytochrome b_6f complex–heavy metals toxicity towards photosynthetic apparatus. *Acta Physiol. Plant.* **2005**, *27*, 61–69.

(59) Lee, D.-Y.; Fortin, C.; Campbell P. G.C. Contrasting effects of chloride on the toxicity of silver to two green algae, *Pseudokirchneriella subcapitata* and *Chlamydomonas reinhardtii*. *Aquat. Toxicol.* **2005**, *75*, 127–135. doi:10.1016/j.aquatox.2005.06.011.

(60) Hiriart-Baer, V.; Fortin, C.; Lee, D.; Campbell, P. Toxicity of silver to two freshwater algae, *Chlamydomonas reinhardtii* and *Pseudokirchneriella subcapitata*, grown under continuous culture conditions: Influence of thiosulphate ». *Aquat. Toxicol.* **2006**, *78*, 136–148. doi:10.1016/j.aquatox.2006.02.027.

(61) Pillai, S.; Behra, R.; Nestler, H.; Suter, M. J.- F.; Sigg, L.; Schirmer, K. Linking toxicity and adaptive responses across the transcriptome, proteome, and phenotype of *Chlamydomonas reinhardtii* exposed to silver. Proc. Natl. Acad. Sci. U. S. A. **2014**, *111*, 3490–3495. doi:10.1073/pnas.1319388111.

(62) Caballero-Díaz, E.; Pfeiffer, C.; Kastl, L.; Rivera-Gil, P.; Simonet, B.; Valcárcel, M.; Jiménez-Lamana, J.; Laborda, F.; Parak, W. J, The Toxicity of Silver Nanoparticles Depends on Their Uptake by Cells and Thus on Their Surface *Chemistry. Part. Part. Syst. Charact.*, **2013**, *30*, 1079–1085.

674 (63) de Gouvion Saint Cyr D.; Wisniewski C.; Schrive L.; Farhi E.; Rivasseau C. Feasibility
675 study of microfiltration for algae separation in an innovative nuclear effluents
676 decontamination process, *Sep. Pur. Technol.* **2014**, *125*, 126–135.

677

678 **Tables**

679

680 **Table 1. Best fit parameters from the refinement of the algae samples exposed to silver**

681 **EXAFS spectra.**

Sample	Ag-S	Ag-Ag	S_0^2, Δe_0, R factor, χ^2_R
Algae exposed to 10^{-3} M Ag^+ (15 K)	0.7(1) S at 2.46(1) Å σ^2 = 0.0057 Å²	3.9(1) Ag at 2.87(1) Å σ^2 = 0.0035 Å²	S_0^2 = 0.9 Δe_0 = 2.53(30) R factor = 0.030 χ^2_R = 0.10
Algae exposed to 10^{-4} M Ag^+ (15 K)	0.7(1) S at 2.46(1) Å σ^2 = 0.0050 Å²	3.6(1) Ag at 2.87(2) Å σ^2 = 0.0032 Å²	S_0^2 = 0.9 Δe_0 = 1.73(24) R factor = 0.019 χ^2_R = 0.19
Algae exposed to 10^{-5} M Ag^+ (15 K)	2.0(1) S at 2.41(1) Å σ^2 = 0. 0048 Å²	0.9(1) Ag at 2.93(1) Å σ^2 = 0. 0059 Å²	S_0^2 = 0.7(1) Δe_0 = 1.94(32) R factor = 0.030 χ^2_R = 0.19

682 σ^2 is the Debye-Waller factor, S_0^2 the passive electron reduction factor, Δe_0 (in eV) the energy
683 shift of the adjustment, R factor is the relative error of the fit versus data, and χ^2_R the reduced
684 χ^2 factor of the statistical chi-square test. Uncertainty is given on the last digit in brackets.

685

686 **Figures**

687

688 **Figure 1.** Ag K-edge normalized XANES spectra of algae exposed to 10^{-6} M, 10^{-5} M, 10^{-4} M
689 and 10^{-3} M Ag^{+} (solid lines) and of Ag reference compounds (Ag_2S for Ag(I) and Ag foil for
690 Ag(0), bolted lines). The spectra have been vertically shifted for clarity.

691

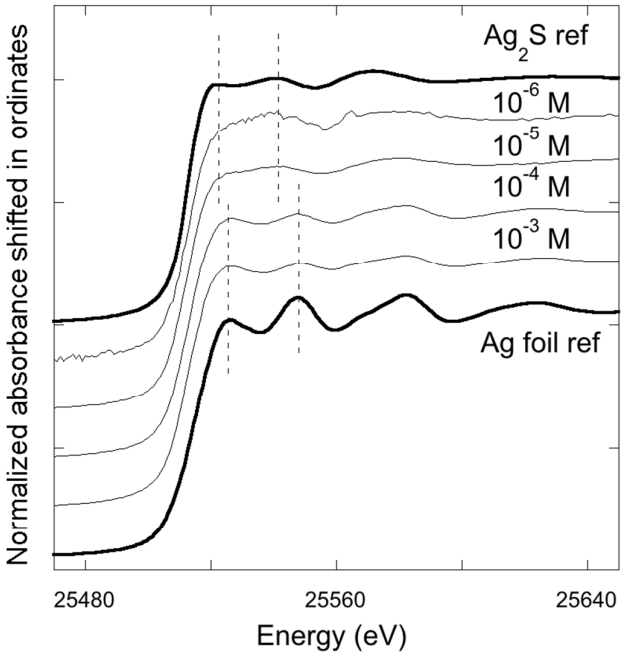

692

693

694 **Figure 2.** (A) Ag K-edge k²-weighted EXAFS spectra and (B) Fourier transforms moduli of
695 algae exposed to 10^{-6} M, 10^{-5} M, 10^{-4} M and 10^{-3} M Ag^{+}. Solid line: experimental data; dotted
696 line: best fit. The spectra have been vertically shifted for clarity.
697

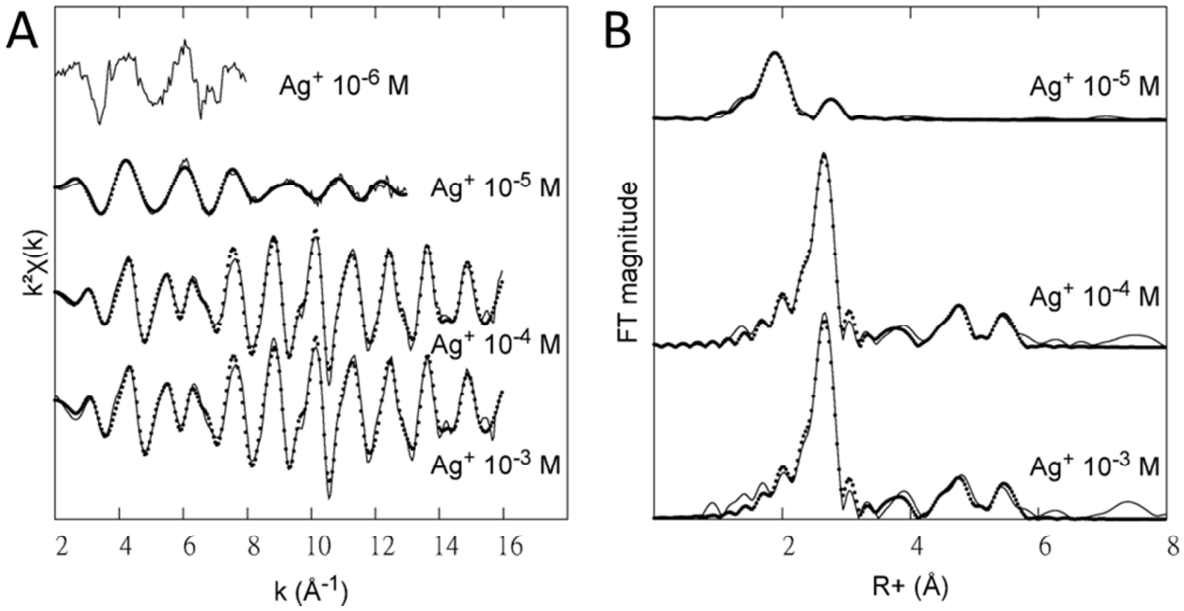

698
699

Figure 3. X-ray diffraction data recorded for (A) solid line: microalgae exposed to 10^{-2} M Ag^{+} in the light, (B) dotted line: microalgae exposed to 10^{-2} M Ag^{+} in the dark, and (C) dashed line: reference sample of microalgae which were not exposed to silver. Vertical unit is arbitrary and spectra were vertically shifted for clarity. The blue lines indicate the peak positions expected for the silver Fm-3m crystallographic phase (face-centered cubic silver crystal) taken from file 00-004-0783 of the ICDD PDF-4 data base. In inset, fit of the (111) peak of the algal sample exposed to 10^{-2} M Ag^{+} in the light assuming a pseudo-Voigt shape function.

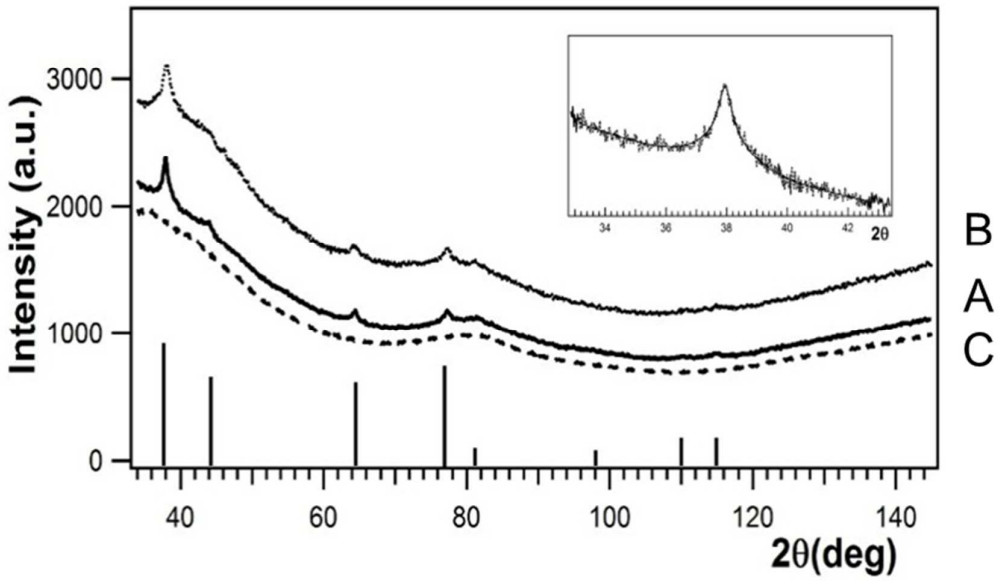

711 **Figure 4.** Nanoparticles localization (black spots) in microalgae exposed to (A, B) 10^{-4} M and
712 (C, D) 10^{-2} M Ag^{+} using TEM. Chl, chloroplast; M, mitochondria; Cyt, cytosol; W, cell wall,
713 S, starch granule; L, lipid vacuole; G, Golgi apparatus; PM, plasma membrane. Arrows point
714 at a few silver clusters.

715

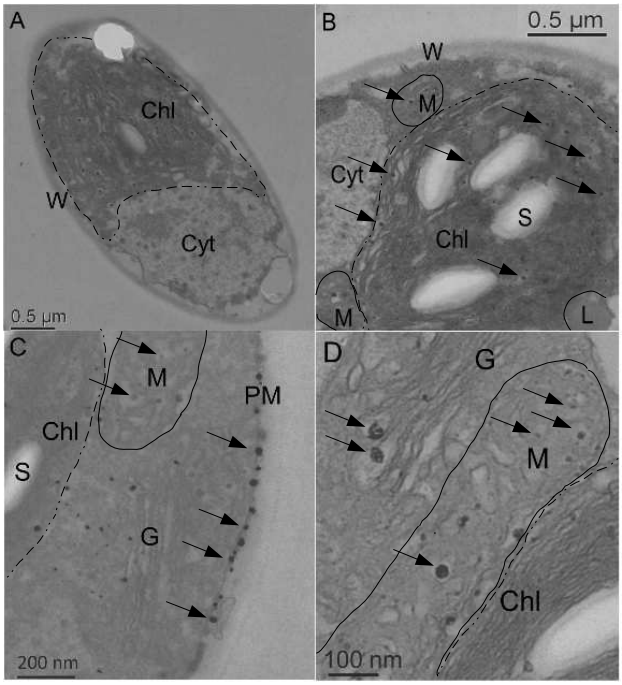

716

717

718

719 **TOC/Abstract Art**

720

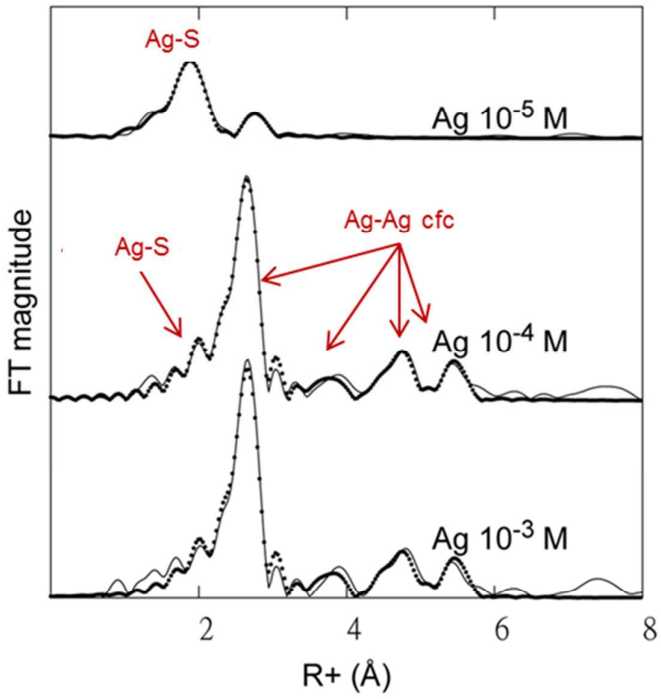

721